Chapter 15

Wave-Surface Interactions

Imaging radars produce high-resolution maps of the radar reflectivity of surfaces. Although these maps resemble pictures of the ground, they are not pictures in the conventional, optical sense at wavelengths $\lambda \sim 0.1$–10μm. Rather, the patterns of brightness and dark in these maps are expressions of the radar scattering properties of the ground cover for $\lambda \sim 0.001$–10 m. Additionally, the illumination in conventional images is almost always either from a range of directions or diffuse emission from the surface itself, whereas since most radars carry the source illuminator, the illumination is antiparallel to the observed scattering. We would therefore like to consider just what properties of the surface are reflected in the radar echoes. In other words, what do we see when we examine radar images?

15.1 Specific RCS: σ^0

The observed brightness in a radar image is typically displayed as proportional to some power of the backscattered energy, and is related the the physical composition of the surface through the strength of the backscatter or the polarization. It also is dependent on the illumination geometry, for usually a surface is brighter when viewed at an angle which is closer to the normal to the mean surface than to grazing incidence, as illustrated in Fig. 15.1.

In addition to questions of viewing geometry, it is also necessary to consider how to characterize the scattering properties of an extended surface. For surface mapping the interesting part includes the variations of RCS with location on the surface. So we characterize not only the scattering from the surface, but how this changes from one point on the surface to another.

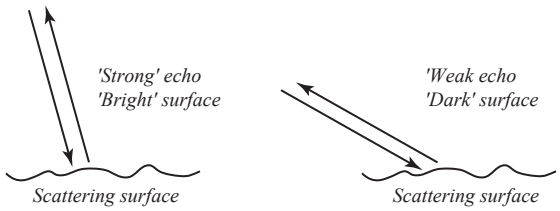

Figure 15.1: Dependence of surface RCS on viewing angle. Same surface may appear bright when viewed at near normal incidence (left) and dark when viewed closer to grazing incidence (right).

In this circumstance our calculation of the RCS of a very large plane is not of much use as i) it applies only for norm incidence and ii) does not address the question of variations. To get at this problem the key concept is that the radar must be able to isolate or distinguish between signals from different parts of the surface. There are several practical ways to do this—as we shall see in later chapters. For now is sufficient to consider the side looking radar method introduced in Section 2.4, in which an narrow beam along track in combination with pulsed range resolution is used to isolate signals from various points within an extended swath along the ground. By use of such methods we can attribute the echo power received at various ranges and points along the SAR flight path to specific areas on the surface in the construction of a radar map or image of the surface. As different radars have different resolution areas on the surface, and even a given radar usually has different surface resolutions at different look angles, we need a uniform measure of the surface scattering that is independent of variations in radar performance. For this purpose we use the *specific, or normalized, radar cross section,*, σ^0 defined as RCS per unit area of the mean scattering surface. This normalized unit will the the same for a given surface viewed with the same geometry independently of the areal resolution of the radar. With this definition the actual RCS for a given area is $\sigma = \sigma^0 dA$, where dA is the resolved area. In calculations of echo power we need only replace σ in Eq. 3.1 with $\sigma^0 dA$. Thus, the received echo power is proportional to σ^0 and embodies both the properties of the scattering surface itself and properties of the imaging geometry. Decoupling of the effects of surface material from those of surface shape and viewing geometry can be difficult and lies at the core of radar image analysis.

The angular variation of backscatter, *i.e.*, $\sigma^0(\theta_{\rm inc})$, where $\theta_{\rm inc}$ is the angle of incidence, usually follows an angular scattering law with the features similar to those shown in Fig. **??**.

The strong enhancement of σ^0 near normal incidence, a transition to a broad slowly varying falloff as θ_{inc} increases, and the marked decrease in scattering strength as $\theta_{\text{inc}} \to 90^\circ$ are typical of backscatter from natural terrains.

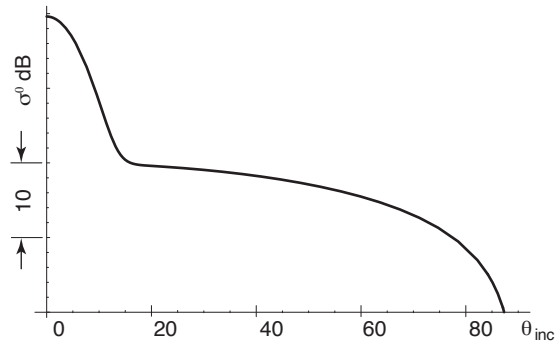

Figure 15.2: Typical backscatter law. Highest RCS occurs at zero incidence and decreases with increasing incidence angle. Change in shape of curve at $\theta_{\text{inc}} \approx 15^\circ$ is result of change in controlling mechanism of scattering.

This dependence of the radar backscatter on angle may be considered as the composite effect of several different scattering processes, some dominant for near-nadir scattering geometries and others dominant at larger incidence angles. The balance between these various processes gives the characteristics of the surface.

Bistatic surface scattering in general has a very different behavior with the strongest echoes occurring in the near forward direction.

In remote sensing applications radar echo intensity depends primarily on the surface shape at the wavelength and longer scale, and only secondarily on the surface electrical properties. That is, surface roughness and topographic shape play a much more important role than variations in dielectric constant, although the latter is result of a rather limited range of material properties found in dry geological materials. Scattering from wet vs. dry surfaces, liquid water, and water ice are principal exceptions where the extreme differences between wet and dry, and liquid and solid states are important factors controlling the RCS. There are, of course, other special cases when ϵ or μ changes dominate, but these occur very infrequently.[1]

[1] An example is the effect of tellurium, which apparently accounts for observations of very strong radar echoes from regions near the tops of mountains on Venus. As a semiconductor tellurium is highly conductive under Venusian conditions; it is the only known material with a phase transition to the solid under the conditions where these radar bright areas are observed.

15.2 Near-Normal Incidence Scattering: Facet models

One of the simpler scattering models is quite important for small angles of incidence. That model is the *facet* surface model which explains the primary properties of near vertical incidence backscatter. In this model the surface is decomposed into small regions, or 'facets,' which lie along the surface. If a facet faces the radar directly, its echo is relatively strong, while if it lies at an oblique angle to the radar look direction its echo will be weaker. When excited by an incident wave, each facet may be thought of as a small antenna illuminating the radar, where the radar cross section is proportional the the radiation pattern generated by the facet, as suggested in Fig. 15.3.

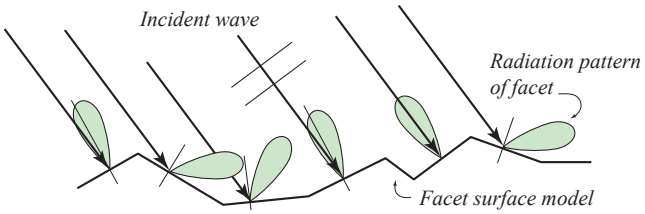

Figure 15.3: Facet scattering model. Surface is approximated by system of flat facets that independently backscatter energy to the radar. Strength of backscattered energy is greatest when facet is normal to radar line-of-sight, and considered negligible when angle between surface normal and line-of-sight exceeds diffraction lobe width of facet.

The return from a facet is greatest when it is illuminated normally, and the total power in the echo can be expressed as the sum of the power from each of the individual facets. Since the power is also related to the Fresnel reflection coefficient of each facet, dielectric constant plays a small role, but the major effect will be from the slope distribution of the surface. Because scattering from the facets is a composite of mirror-like reflections, this type of scattering is referred to as *quasi-specular*, in order to distinguish it from 'specular' reflection of a large smooth plane. Quasi-specular scattering is common to near-vertical incidence observations of lightly vegetated regions of the earth, as well as the moon and terrestrial planets.[2]

For most surfaces, the probability that a facet has a slope greater than a few degrees is

[2]Mercury, Venus, Earth, and Mars. Scattering from the icy polar regions of Earth and Mars is distinctly not quasi-specular, however.

quite small, so facet models would predict little returned power for $\theta_i \geq 15$–$20°$. For some surfaces, such as water, incidence angles θ_i greater than 1–2° are rare. Hence a smooth surface, such as most water surfaces, will exhibit high backscatter within only a narrow region around zero incidence, while a rougher surface with much greater average slopes, such a dune fields, will evidence backscattered energy over a much wider range of θ_{inc}. This phenomena allows us distinguish between smooth and rough surfaces by the width of the quasi-specular part of the σ^0 curve. Two curves of σ^0 shown in Fig. 15.4 illustrate the the variation in form that the facet model predicts for varying roughness.

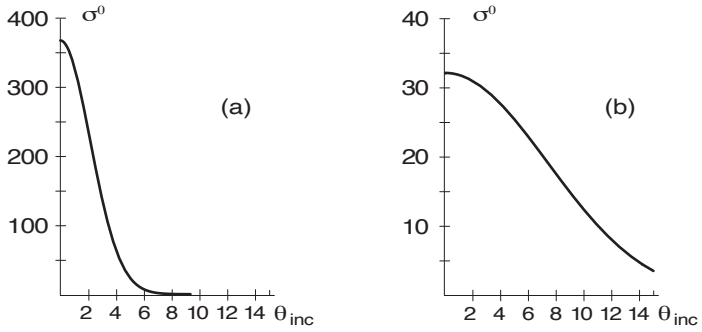

Figure 15.4: Scattering from Smooth and Rough Surfaces. Facet scattering model predicts that for a smooth surface most of the backscattered energy is observed primarily at small incidence angles (a), while rougher surfaces produce significant returns at higher angles (b). Curves are drawn for Gaussian distribution of surface slopes with 3°and 10° in panels (a) and (b), respectively. Note 10:1 difference in vertical scales.

15.3 Moderate Incidence Scattering: Perturbation models

For larger incidence angles, the number of facets facing the radar with near normal incidence is very small, with the result that other effects scattering processes dominate the radar return. Several models are commonly invoked to model σ^0 for incidence angle θ_i greater than about 20°, the most common of these models being based on *Bragg scattering*, where certain spectral components of the surface height $\xi(x, y)$ couple strongly to the incident wave.

For the Bragg scattering model, we consider a surface as broken up into a large-scale, faceted component as before plus a residual small-scale roughness component (see Fig. 15.5). This decomposition keeps the amplitudes of the roughness component small, so that perturbation

methods may be used to evaluate scattering behavior. This is not always required, though, if specialized numerical methods are used to calculate the scattering properties. We find the small-size restriction helpful in our brief analytical treatment, and adopt it here.

Figure 15.5: Two-scale model with facets. Rough surface is decomposed into two components: (i) a large-scale facet model that describes the overall shape of the surface plus (ii) a small-scale roughness component with low values of residual amplitude.

We consider the faceted component in a moment. First examine the small scale roughness component and break it up into surfaces of differing spatial frequency using Fourier analysis, as shown in Fig. 15.6, where each of the Fourier components is relatively small-scale in amplitude.

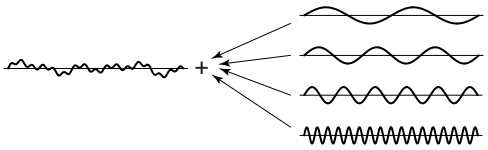

Figure 15.6: Fourier decomposition of surface roughness. Small-scale roughness surface may be decomposed into many components of differing spatial frequency. Relative spatial frequencies in figure are 2, 3, 11/2, and 33/2 cycles/unit length; corresponding amplitudes of composite surface are 1,1,1, and 0.75, respectively, where the component with the lowest spatial frequency (2 c/l) substitutes for facets in the previous model.

Usually the analysis requires that the rms height h of the roughness component be less than $\frac{\lambda}{8}$ in amplitude, which is why we removed the large-scale facets before the decomposition. We will put the effects of the large-scale surface shape back in after considering the small-scale surface scattering.

In Bragg scattering models only one Fourier component of the surface shape, the component for which the distance Λ as shown in Fig. 15.7 is equal to $\frac{\lambda}{2}\sin\theta_i$, will result in significant

backscatter. As suggested by the figure, the return echoes from each cycle of this component of the surface height distribution add up in phase. In other words, we assume that the incident wave, when projected onto the surface, is resonant with this single component of the surface spectrum. Therefore surface variations at this spatial frequency are dominant in affecting the amount of reflected energy. All other terms of the surface height distribution will not resonate, and provide very little return signal.

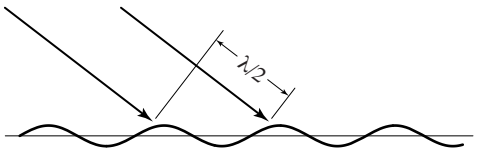

Figure 15.7: Bragg scatter model. This model is based on strong coherent reinforcement of backscatter by the spatial component of the surface roughness for which the projected incident wave resonates.

Scattering properties of the Bragg model can be evaluated formally by use of perturbation methods, leading to an expression of the normalized cross section as a function of surface electrical and physical parameters as σ^0 as,

$$\sigma^0{}_{\text{pol}} = 8k^4h^2\cos^4\theta|\alpha_{\text{pol}}|W(2k\sin\theta) \tag{15.1}$$

where α_{pol} depends on the wave polarization and $W(\cdot)$ is the power spectrum of the surface. The $\cos^4\theta$ term expresses the incidence angle dependence of the cross section for fixed $W(\cdot)$. It is clear from eq. 15.1 that only the component of the surface spectrum meeting the Bragg condition affects the reflectivity.

15.4 Discrete Scatterer Models

Another model valid over a wide range of incidence angles, but most useful at larger angles, simply considers each resolved area to consist of a finite set of discrete scatterers, which are considered as point scatterers. Echoes received from each scattering point on the surface within

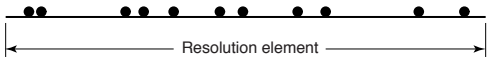

Figure 15.8: Discrete surface scattering model. Model represents surface as a collection of independently scattering elements, with the total echo simply the coherent sum of all of the individual echoes.

the resolved area add coherently, but the randomness of the locations introduces a statistically random phase to the composite signal from the resolved area, as we saw before when we evaluated the cross section of complex objects and aggregates of multiple scatterers. From Eq. 5.55, taking each scattering point to have the same scattering strenth, $\sigma_{\rm sp}$, and letting N represent the number of scattering points per unit area on the ground, we can write down directly that,

$$\sigma^0(\theta) = N \cdot \sigma_{\rm sp} \cdot \cos\theta_{\rm inc} \tag{15.2}$$

where the obliquity factor, $\cos\theta_{\rm inc}$ is needed to account for the reduction in incident power per unit area of the illuminating wavefront, Fig. 15.9.[3] Eq. 15.2 holds for isotropic scattering elements. If, on the other hand, the reradiation patterns of the scatterers are not isotropic, the proper radiation pattern for each scatterer should be substituted. For horizontal dipole scatterers lying in the plane of scattering the radiation pattern is $\cos^2\theta_{\rm inc}$, in which instance the composite scattering function becomes,

$$\sigma^0(\theta) = N \cdot \sigma_{\rm dipole} \cdot \cos^3\theta_{\rm inc} \tag{15.3}$$

Both of these models, Eqs. 15.2 and 15.3, fall off with incidence angle even more slowly than the Bragg model, and are used for very rough surfaces where the small-height restrictions of the Bragg model are exceeded.

[3]There is a subtle point here. The obliquity correction strictly applies only when the scattering surface is treated as a continuum. Scattering from a very loose collection of discrete objects on the surface would not be expected to experience the wave projection effect until $\theta_{\rm inc}$ is greater than some treshold value. To understand this, consider an instance with only a few scattering points in a particular surface versus a continuously scattering surface.

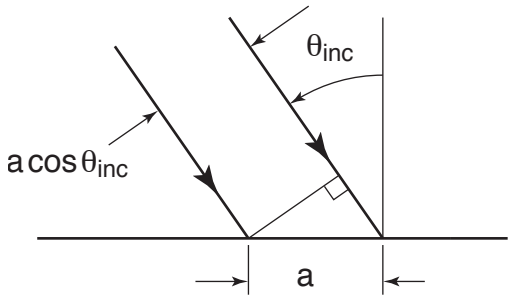

Figure 15.9: Wavefront projection on mean scattering surface. Two rays with angle of incidence $\theta_{\rm inc}$ separated by a distance a along the surface surface are separated by only $a\cos\theta_{\rm inc}$ when measure perpendicular to the wavefront. Thus, the power per unit area of surface decreases decreases with increasing $\theta_{\rm inc}$ as a decreasing total power, $\mathcal{S}_{\rm inc}a\cos\theta_{\rm inc}$, is distributed over a fixed surface area.

15.5 Slope Modulation: Brightness effects from topography

We now consider the effects on the backscatter function $\sigma^0(\theta_{\rm inc})$ of large scale variations of the surface, such as those due to topographic variations on the surface. We begin by considering a typical composite backscatter model, such as that shown in Fig. 15.2 above. Suppose that we are imaging a topographic hill, which we show schematically in Fig. 15.10(a). We presume that the surface shown in Fig. 15.10 represents the large scale average of a scattering surface with a known scattering law. In order to evaluate the brightness of different regions of this surface, we first determine the local incidence angle at each point on the large scale surface. These angles are identified in Fig. 15.10(b), where the smallest incidence angle is associated

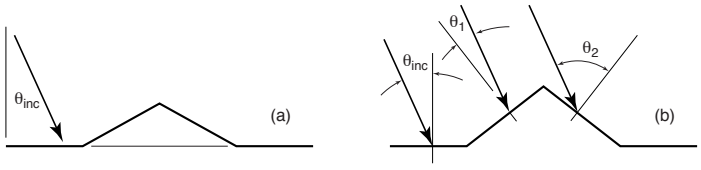

Figure 15.10: Surface slope modulation of RCS. Topographic hill has smallest angle of incidence on leading edge, which appears as the brightest area in the image. The back side of the hill is the darkest region, with flat slopes intermediate in brightness.

with the front side of the hill, the largest incidence angle with the back side of the hill, and intermediate angles correspond to the horizontal surfaces. Recall that the backscatter function typically is greatest for small angles, and decreases monotonically, Fig. 15.2. Consequently, the topographic hill feature appears brightest on the side toward the radar and darkest on the side away form the radar. This slope-dependent shading effect makes even relatively subtle changes in topography quite pronounced in a radar intensity image.

15.6 Surface Roughness Variations

Now examine the affect on the scattering of radar signals arising from changes in the roughness of the scattering surface. Increasing the surface roughness has two effects on the radar echoes that can be inferred from the discussions on facet models and on Bragg scattering in the previous sections. First, increasing roughness spreads the reflected energy from facets over a larger range of scattering angles because an increase in roughness is usually accompanied by an increase in the width of the surface slope distribution. Second, Bragg scattering intensity increases as it is directly proportional to the square of the rms height of the surface, Eq. 15.1, thereby increasing the contribution to the RCS from small-scale surface roughness.

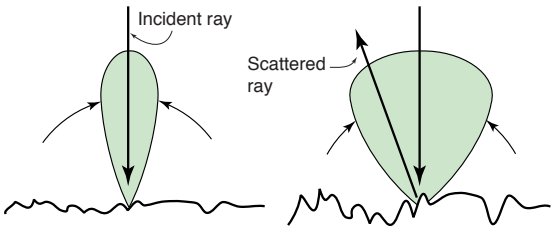

Figure 15.11: Effect on RCS of varying surface roughness. Smooth surfaces result in backscattered energy concentrated in a relatively narrow scattering lobe, while rougher surfaces spread the same incident energy over a wider range of angles. Strength of scattering lobes here are the same for clarity. Generally, for the same surface materials, maximum strength of scattering in wider lobes will be less than that of narrow lobes.

These two physical effects tend to result in backscattered energy that is more concentrated in a single narrower scattering lobe for the smoother surfaces, as suggested by Fig. 15.11. The image for a rougher surface will be darker for small incidence angles and brighter for large incidence angles than for a smoother surface. Sample comparative plots of the backscatter

intensity function are shown in Fig. 15.17. Note the cross over of the $\sigma^0(\theta_{\text{inc}})$ curves a $\theta_{\text{inc}} \simeq 6°$. Rougher surfaces appear brighter for θ_{inc} larger than the cross over angle, while smoother surfaces are brighter for θ_{inc} less than the cross over angle. Observe that because topographic

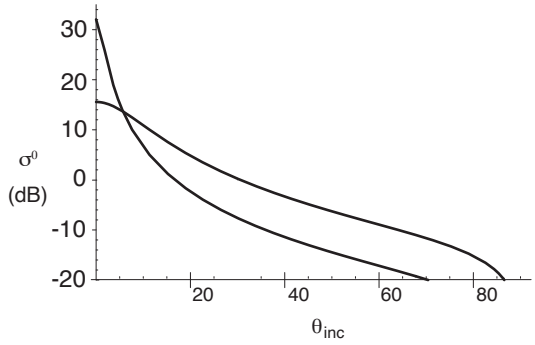

Figure 15.12: Variation of backscatter function with surface roughness. Backscatter function of smooth surface is more peaked near zero and lower at higher incidence angles than the backscatter function of a rougher surface. Figure depicts surfaces with nominal RMS slopes of 1/6 and 1/40 for the relatively flat and steep curves, respectively. Computation is based on the Hagfors' Law.

shading depends on the slope of the cross section as a function of incidence angle $\frac{\partial \sigma^0(\theta)}{\partial \theta}$, the shading effect is strongest in smoother areas viewed at near-normal incidence than in rougher areas viewed at moderate and higher angles of incidence.

Scattering from vegetation can be thought of either as scattering from an extremely rough surface, or as resulting from the previously-described discrete element scattering (*v.* Fig. 15.13). Either of these models predict only slight dependence on the normalized cross-section σ^0 on angle of incidence. Thus, scattering from a distributed canopy that is very dense. Backscattering from the Amazon rain forest, for example, has little dependence on θ_{inc}. In fact, the near independence of σ^0 on θ_{inc} for scattering from dense, uniform vegetation makes such areas useful for antenna pattern measurement and calibration (*v.* Fig. 15.14 for sample σ^0 plots for dense vegetation).

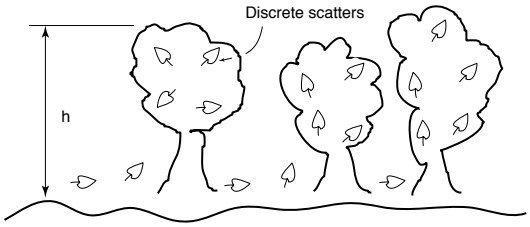

Figure 15.13: Volume scattering by vegetation. Vegetation layer can be viewed as a collection of discrete scatterers in volume of thickness h. Such layers exhibit little angular dependence.

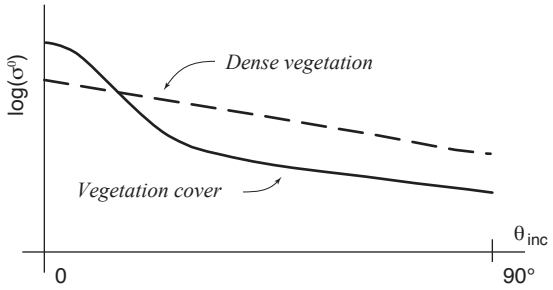

Figure 15.14: Use of vegetation for radar calibration. Regions of thick vegetation are often used for calibration of radar systems as their cross section is less dependent on imaging geometry than other regions. Hence small errors in such factors as incidence angle or antenna beamwidth are less than they would be if RCS variations were more rapid, as is typical of most scattering surfaces.

15.7 A distribution of discrete scatterers

It is said that radar scattering from a surface or volume is dominated by the echoes from objects similar in size to the radar wavelength. In practice this rule of thumb is often correct; it follows as a consequence of the interplay between the variation in scattering efficiency of objects with size and their natural size distribution. We can understand why this is so if we first examine the relative cross section of particles of various sizes.

We have seen that the G.O. RCS of large spherical objects equals the object's projected area, Section 4.2.1, p. 78. Figure 15.15 shows the variation in RCS of conducting spheres normalized by the projected area for a wide range of particle size, for spheres with radius of

about $\lambda/30$ and larger. This ratio is referred to as the *scattering efficiency.* For scatterers caption expan

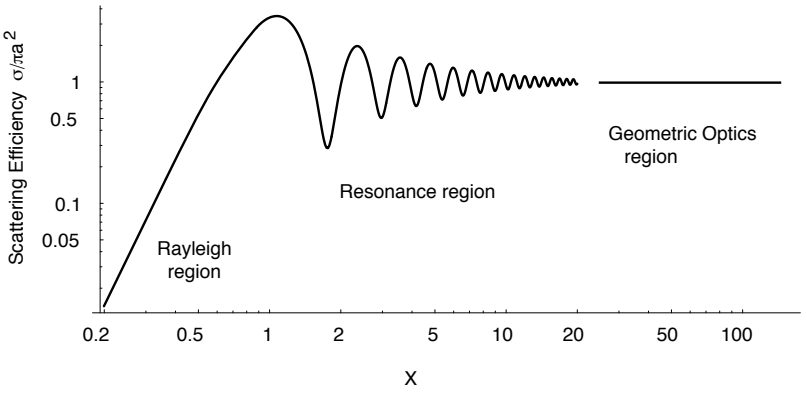

Figure 15.15: Scattering efficiency of a sphere. RCS normalized by projected area ($\sigma/4\pi^2$). Size of sphere is expressed in terms of the size parameter, $X = 2\pi a/\lambda$, where a is the radius, λ the wavelength. Three distinct scattering mechanisms are important in this plot: (i) Rayleigh scattering for small particles of any shape, $x \leq 1$; (ii) resonance scattering for sizes comparable to a wavelength, $1 < x \leq 10$; and (iii) geometric optics scattering for large objects, $x < 10$. Boundaries of resonance and geometric optics regions are indistinct and depend on details of object material and shape. Scattering behavior illustrated by a sphere is representative of scattering from many objects.

of radius significantly less than $a/\frac{\lambda}{2\pi}$, *i.e.*, less than about 1 wavelength in circumference, the scattering efficiency is proportional to a^4, while it is essentially unity for much larger objects.

We call the region of sizes where scattering efficiency decreases quickly with decreasing size the Rayleigh region, because Rayleigh (small-particle) scattering dominates here.[4] The region for which the scattering efficiency is essentially unity is the geometrical optics region, as the geometrical optics result holds. In between is the resonance region, where behavior is more complicated and forms a transition between the two other regions.

For most classes of natural objects, the number density of scatterers of various sizes follows a power law distribution,

$$N(a) \propto a^{-n} \tag{15.4}$$

[4]Rayleigh scattering is an important regime for many disciplines. Scattering cross section for *any* particle with characteristic dimension $\ll \lambda$ is proportional to a^6/λ^4. That is, the scattering of small objects varies as V^2/λ^4, where V is the volume.

where a is the characteristic size and the exponent n is the power law index. When presented on log-log coordinates n is the slope of the resulting straight line, as shown in Fig. 15.16. The value of the index has a large possible range, but for most problems of interest here, $2 < n < 4$.

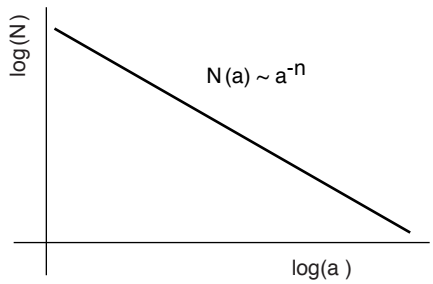

Figure 15.16: Power-law distribution function. Natural surfaces and volumes usually possess a distribution of size scales that is well-represented by a power law.

When we have a collection of independent scatterers of different sizes, we estimate the total cross section by first evaluating the individual cross section of each particle and then adding up the results. The curve in Fig. 15.15 tells us how to weight each of the geometrical cross sections for the various scatterers when we sum the total cross section.

As an illustration, consider the distribution of scatterers forming a tree. The tree is composed of many objects of differing size, from small needles and leaves up to the large trunk. On most trees there are many more leaves than trunks and branches. We can create a typical scattring model 'tree' by tabulating the size and number density of each component part. Table 15.1 gives results for an r^{-3} tree, where r is the characteristic dimension of the part, as that is the approximate power law expressing the change in number density for a given change in scatterer size on a reasonable tree. Other 'trees' or other ensembles may be modeled on the basis of different power laws.

In order to calculate the radar cross section, we must first determine the physical and radar cross sections of each tree element. We first assume that we are studying the r^{-3} tree with a radar operating at a wavelength of 12.5 cm, with the results given in Table 15.7, which gives results for 'Total Area' and 'RCS' corresponding to the part types, sizes, and numbers in

Tree Part	Equivalent Size	Number
Trunk	100 cm	1
Large Branches	50 cm	8
Small Branches	25 cm	64
Twigs	$12\frac{1}{2}$ cm	512
Leaves	$6\frac{1}{4}$ cm	4096

Table 15.1: Equivalent Size and Number of Scattering Objects for an r^{-3} Tree. Table gives numbers of various parts for power law tree with index $n = 3$. As most actual trees have only a single trunk, the table begins with this value. Sizes of other parts are arbitrarily set by powers of two, for convenience. This table created for illustration only.

Table 15.1. In calculating the RCS we have assumed that the RCS of each tree part is equal to its area if the size parameter for that part is greater than unity, *i.e.*, $X > 1$, and that the RCS follows the Rayleigh Law for $x \leq 1$. Study of Fig. 15.15 shows that this approximation is accurate except in the limited range of size parameter $0.5 < X < 5$, and that the maximum errors are not important for purposes of illustration.

Tree Part	Number	Total Area	$\lambda = 12.5$ cm Total RCS	$\lambda = 25$ cm Total RCS
Trunk	1	π	π	π
Large Branches	8	2π	2π	2π
Small Branches	64	4π	4π	4π
Twigs	512	8π	8π	$\frac{\pi}{8}$
Leaves	4096	16π	$\frac{\pi}{4}$	$\frac{\pi}{256}$

Table 15.2: Area and Total RCS of tree parts ($\lambda = 12.5, 25$ cm). Total area is obtained by taking the projected area as πa^2 for each tree part and multipling the result by the number of parts. Estimates of RCS are based on a two part approximation to Fig. 15.15 with transition at $X = 1$ (*v.* text). Note that 'Leaves' are in the Rayleigh scattering regime $X \leq 1$ while larger parts have $X > 1$.

The combined effect of a size distribution that favors smaller objects and a scattering efficiency that discounts the return from objects smaller than a wavelength in size leads to the greatest contribution from the wavelength-size objects. For $\lambda = 12.5$ cm the peak contribution to RCS comes from twigs, whose physical sizes are comparable to the radar wavelength. If instead we use a radar with a longer wavelength of 25 cm-λ, we obtain different values for the

cross section of each set of component parts – at 25 cm–λ the greatest contribution to the RCS is from the small branches, which are twice the size of the twigs. Once again the radar echo is dominated by objects comparable to a wavelength in size. Use of several different radar wavelengths allows us to probe objects at different size scales.

The assumption of an r^{-3} is convenient for computation but is not necessary for the result that the strongest contributors are roughly λ-size. There is a range of indices for which this result obtains, but it is limited. We summarize the effects of changing n in Table 15.7.

Power Law	Results for Total RCS
r^{-1}	Large objects dominant
r^{-2}	All objects larger than $X \approx 1$ contribute equally
r^{-3}	λ-size objects dominant
r^{-4}	Strong selection of $r \approx \lambda$ size objects
r^{-7}	Smallest objects in distribution dominant

Table 15.3: Summary Behavior of Aggregate Scattering for Power Law Distributions. Contributions of various size objects to total RCS depends on the relative numbers in each size range, weighted by the scattering strength for each size. $n = 2$ results in a uniform contribution for large objects because product of numbers per size unit and area of each size is constant.

Of course a real tree does not exhibit an infinitely extended r^{-3} power spectrum. There are no scatterers larger than the trunk, leading to a large-scale cutoff, and if the small objects are placed very close together they exhibit bulk properties which can change the results of the simple scattering calculations here. But this model is illustrative and is accurate enough for some purposes. Therefore, we would expect most vegetated surfaces to look different to different wavelength radars.

An implicit assumption for this type of model is that each object in the distribution scatters independently of all the rest. This same assumption applies in the analysis of scattering from multiple objects in Section 5.5. This is valid with the volume density of the objects is low and/or the scattering from individual objects is weak. Certainly when objects are more closely spaced that about 10 λ or 10 radii they begin to interact electromagnetically regardless of other considerations, and the assumption of independent scattering fails.

As it happens scattering from rough surfaces also varies with wavelength, with the apparent or 'radar' roughness generally decreasing as the wavelength is increased. Although the power

law example provides an important insight for collections of discrete scatterers, the problem of wavelength dependence of scattering from rough surfaces is much more complex, and remains an area of active research.

15.8 Some Scattering "Laws"

Characterization of the relationship between surface roughness and electromagnetic scattering is difficult for all but the simplest of surfaces. No exact solutions to Maxwell's equations valid for all wavelengths exist even for easily described deterministic surfaces such as harmonic undulations or uniform square waves, although limited solutions applicable for a restricted range of wavelengths are available. Restricted solutions also exist for stochastic surface models. In some instances a statistical solution is more readily obtained than is a deterministic result, as a result of simplifications associated with the averaging process.

With the understanding that exact solutions are unusual, it is useful to be aware of a few scattering "laws" that provide representative results for various surface types and which are also in wide use. Each of these is a simple analytical formula describing how the normalized radar cross section σ^0 depends on incidence angle θ. Four such laws are the exponential, the Gaussian, the Hagfors law, and the 'cosine-to-the-n.' The first three of these are often referred to quasispecular scattering laws, in which the response is computed using physical optics and various assumptions on the probability distributions of surface height and slope. These approximations are most accurate in the near-specular direction, that is, near normal incidence ($\theta = 0$) for backscatter and near the forward specular direction for bistatic geometries. The cosine-to-the-n approximation is used most often when volume scatter of one sort or another is significant. Many surfaces may be approximated by one of these laws for a subset of incidence angles and another for the remaining incidence angle range. All of these have been in analytical use as models for specifying engineering performance in radar designs.

15.8.1 Quasispecular scattering

Quasispecular, or near-specular, direction scattering laws derive from a physical optics approach called the Kirchhoff approximation. Under this approximation each point on the scattering surface is treated as a point on an infinite tangent plane made up of same material as the surface under study. Surfaces of sufficiently small roughness, with limited surface slope and

height distributions, satisfy boundary conditions mathematically, however it is common practice to use the approximations beyond their formal limits as scattered power measurements have often been observed empirically to follow the predicted angular dependence as closely as other means for modeling the echo. Using several well-defined distributions for height and slope variations yields many different scattering functions, some of which will match measurements better than others.

A criterion for quasispecular scattering is that the surface is smooth, which under the Rayleigh criterion means that the root-mean-square height h_{rms} is such that

$$h_{rms} < \frac{\lambda}{8\cos\theta} \tag{15.5}$$

The rms height h_{rms} is the first descriptor of the surface under observation. As noted above, even if the rms height exceeds this value, measurements still tend to follow the derived angular dependence, so that these laws are more robust than the mathematical assumptions would imply.

The second descriptor needed is the roughness in the horizontal direction, rather than in the vertical direction of h_{rms}, and is usually quantified as the surface autocorrelation function $C_f(R)$. This function will possess an autocorrelation length, R_0, the distance at which the autocorrelation function falls by a factor of e^{-1}.

The rms height and autocorrelation functions are related to the distribution of slopes $p(\theta)$. The slope distribution too is characterized by an rms value, s, which would be zero for a perfectly flat surface and yields a finite value for surfaces with realistic roughnesses. The rms surface slope s depends on the autocorrelation function and the rms height,

$$s = h_0\sqrt{-2C_f(0)''} \tag{15.6}$$

where $-2C_f(0)''$ is the second derivative of the autocorrelation function, evaluated at $R = 0$.

The scattered power depends not only on the distributions of slopes and heights, but also on the dielectric properties of the surface. Because the quasispecular approximation takes scattering as resulting from a plane tangent to the surface, and only planes normal to the wavefront contribute, we can compute the scattered power from a perfectly conducting surface of the same shape as the surface under study, scaled by the Fresnel reflection coefficient ρ of

the surface material. For a surface of bulk dielectric constant ϵ we can compute ρ from

$$\rho = [\frac{\sqrt{\epsilon}-1}{\sqrt{\epsilon}+1}]^2 \tag{15.7}$$

We will also find it convenient to parameterize the angular extent of the backscattered lobe. which we will denote C. Not to be confused with the autocorrelation function of similar notation, traditionally C has been defined as

$$C = \frac{\lambda^2 R_0^2}{16\pi^2 h_{rms}^4} \tag{15.8}$$

The roots of this definition are historical, but the inverse square root of C has often been taken to be the rms surface slope:

$$s = \frac{1}{\sqrt{C}} \tag{15.9}$$

Typical assumptions for both the surface heights and autocorrelation functions are either exponential or Gaussian forms, with different combinations resulting in different scattering functions. Tabulating exponential and Gaussian forms for each,

$$p_e(h) = \frac{1}{h_0} \exp[\frac{-h}{h_0}] \tag{15.10}$$

$$p_G(h) = \frac{1}{h_0\sqrt{2\pi}} \exp[\frac{-(h-\bar{h})^2}{2h_0^2}] \tag{15.11}$$

$$C_{fe}(R) = \exp[\frac{-R}{R_0}] \tag{15.12}$$

$$C_{fG} = \exp[\frac{-R^2}{R_0^2}] \tag{15.13}$$

where as before $p(h)$ is the pdf of heights and $C_f(R)$ is the surface autocorrelation.

Using these distributions, we can compute the rms slope for the exponential correlation function as

$$s = h_0\sqrt{\frac{1}{R_0 R_{min}}} \tag{15.14}$$

where R_{min} is the minimum horizontal size scale of the surface that meaningfully contributes to scattering. This may seem confusing, but it is just stating that the echo power is not dependent on scatterers much smaller than a wavelength, as we saw above in the discussion on scattering from trees. R_{min} is customarily taken such that the rms slope s is equal to the width parameter

C.

The result for the Gaussian correlation function is simpler,

$$s = h_0 \frac{\sqrt{2}}{R_0} \tag{15.15}$$

At this point we are ready to examine the exponential, the Gaussian, the Hagfors laws. Each follows from a particular combination of height, slope, or correlation distribution.

Exponential Law

The exponential law follows if we use an exponential function for both the height and slope distributions:

$$\sigma^0{}_e(\theta) = \frac{3\rho C}{\cos^4\theta} \exp(-\sqrt{6C}\tan\theta) \tag{15.16}$$

Gaussian Law

For the Gaussian law, we use a Gaussian distribution for both the heights and the autocorrelation function:

$$\sigma^0{}_G(\theta) = \frac{\rho C}{\cos^4\theta} \exp(-C\tan^2\theta) \tag{15.17}$$

Hagfors Law

If we instead use a Gaussian distribution for the heights and the exponential autocorrelation function, we obtain Hagfors law:

$$\sigma^0{}_H(\theta) = \frac{\rho C}{2}(\cos^4\theta + C\sin^2\theta)^{3/2} \tag{15.18}$$

We can compare these different forms for normalized radar section σ^0 by plotting them for similar sets of surface parameters. We let the Fresnel reflection coefficient be unity, wavelength 10 cm, h_{rms} 1 cm, and s 8 °. (These selections imply that C=51.3, and $R_0 \approx 9$ cm, implying that the surface decorrelates over a distance comparable to the wavelength.)

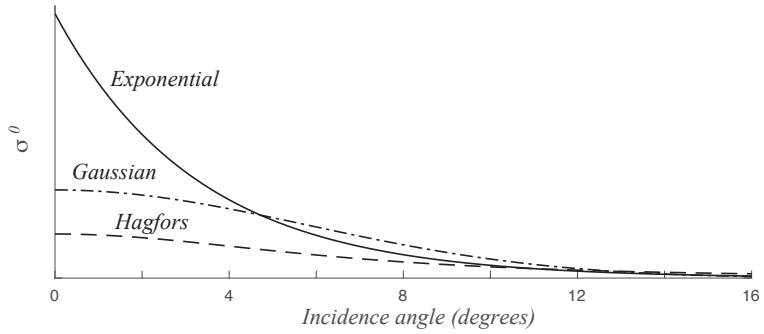

Figure 15.17: Quasispecular models. Normalized radar cross section σ^0 as a function of incidence angle for exponential, Gaussian, and Hagfors Laws. These models are valid for near-normal incidence, note that the range of angles plotted is for $\theta < 16°$. These curves are computed assuming $\lambda = 10$ cm, rms surface height $h_{rms} = 1$ cm, and rms slope $s = 8°$.

15.8.2 Diffuse Scattering: Cos^n Law

The quasispecular laws all derive from considering backscatter by facets normal to the incident wavefront, and hence are only valid for angles corresponding to physically realizable angles of repose. In other words, because local slopes rarely exceed 10°- 20°, these functions predict very little return from larger angles of incidence. But we in fact measure quite large signals at these larger angles, so other mechanisms may be in play. Scattering from large angles is often referred to as diffuse scattering, as it can represent, for example, multiple scattering events that still return energy to the illuminating radar. Analytical solutions for diffuse scatter can be very complex and specialized, so it is common practice to characterize these with a combination of analytical modeling and empirical observation.

Perhaps the most common diffuse scattering "law" is the $\cos^n \theta$ form, whose shape is such that it falls off slowly over the full range of $0 < \theta < \frac{\pi}{2}$. Observed values for the exponent n range from unity, corresponding to isotropic scatter from the surface, to 2, which represents a surface scattering according to the optical remote sensing derived Lambert's Cosine Law, where energy scattered from a surface is concentrated with cosinusoidal dependence. Coupled with the cosine inherent in the definition of σ^0 whose units are m^2/m^2-surface, the exponent assumes a value of 2. Natural diffusely scattering surfaces rarely exhibit exponents greater than 2. The simplest form, then, for a diffuse scattering component, is

$$\sigma^0 = A \cos^n \tag{15.19}$$

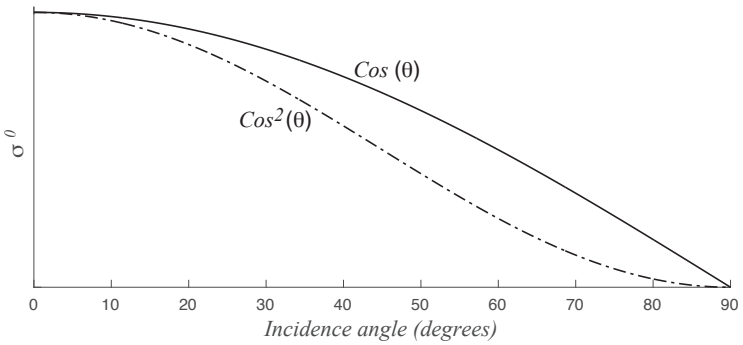

Figure 15.18: Cos^n models. Normalized radar cross section σ^0 as a function of incidence angle for $\cos^n\theta$ models. Depicted here are results for isotropic scatter ($\cos\theta$) and Lambertian scatter ($\cos^2\theta$).

Real surfaces are generally more complex than these simple models might indicate. It is useful to combine one or more models to represent scatter accurately over a large angular range. For example, we might use Hagfors Law for small incidence angles and a diffuse component for the larger angles, with the total scattering function being a weighted sum of the two models (see Fig. 15.19).

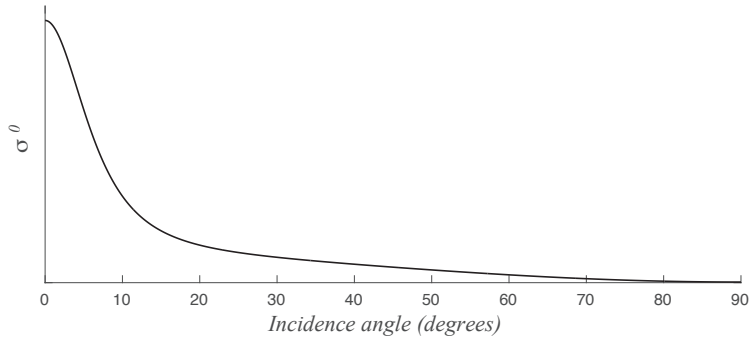

Figure 15.19: Composite model. Normalized radar cross section σ^0 as a function of incidence angle for composite surface with both quasispecular and volume scattering components. Plotted here is sum of Hagfors and $\cos^2\theta$ models.